Influence of the electrolyte composition on the electrochemical dissolution behavior of forged Inconel 718

Mariem Msakni Malouche, Nicolas Stein, Janvier Lecomte, Clotilde Boulanger, Mickael Rancic

Influence of the electrolyte composition on the electrochemical dissolution behavior of forged Inconel 718

Mariem Msakni Malouche [a, b], Nicolas Stein [a*], Janvier Lecomte [b], Clotilde Boulanger [a], Mickael Rancic [b]
[a] *Université de Lorraine, CNRS, IJL, F-57000 Metz, France*
[b] *Safran Aircraft Engines, F-91100 Corbeil-Essonnes, France*
[*] *corresponding author*

Abstract

The forged Inconel 718 anodic dissolution at fixed applied current density was investigated in different nitrate sodium based electrolytes, namely in $NaNO_3$ 8 wt.% and 20 wt.%, in $NaNO_3$ 15 wt.% + $NaClO_3$ 20 wt.% and in $NaNO_3$ 20 wt.% + sulfosalicylic acid 2 wt.%. The analysis of the different anodic products on the surface sample, by X-Ray diffraction, Scanning Electron Microscopy and Energy Dispersive X-ray spectroscopy, revealed a presence of oxides mainly constituted of Nb and Ti oxides and a smaller amount of γ'' phase precipitate than in raw material. Inductively Coupled Plasma (ICP) analysis has shown that the main elements of the matrix (Fe, Cr, Ni) are soluble in all tested electrolytes while Nb content is below the detection threshold in pure $NaNO_3$ electrolyte and in 15 wt.% $NaNO_3$ + 20 wt.% $NaClO_3$. However, in presence of sulfosalicylic acid, acting as chelating agent, the amount of anodic products on the surface sample has considerably reduced comparatively to other tested electrolytes and Nb was detected by ICP analysis as additional element in the electrolyte. Therefore, this work shows that the Inconel 718 super alloy can be homogenously anodized by the use of an adapted chelating electrolyte, opening up possibilities for efficient electrochemical machining processes.

Keywords

Anodic dissolution, surface products, oxide film, chelating agent, Inconel 718.

Introduction

Due to its particular mechanical and thermal properties, nickel based alloys such as Inconel 718 are widely used for aerospace industry. They are known to be among the most difficult to-cut-materials (1), so that conventional machining processes such as milling, drilling and turning have low efficiency and are hard to proceed (2).

Because of its ability to generate high quality surfaces and to reproduce complex shapes, electrochemical machining (ECM) appears to be an interesting alternative to machine those alloys. The main advantage of this non-conventional process is that there is no tool wear (3) due to the absence of physical contact between the work piece and the work tool. In addition, no stress is generated in the sample during the process and then no additional process steps are needed (4). To achieve higher machining accuracy and surface quality, the derivate technology, Pulse ElectroChemical Machining (PECM), is appropriate due to low inter-electrode gap and a short pulse current applied contrary to classic ElectroChemical Machining (High inter-electrode gap and continuous current)

For both ECM and PECM, the generation of anodic film and the understanding of the related physical and chemical phenomena have been largely explored for stainless steel and iron (4) (5) (6) (7) (8). On the contrary, to the best knowledge of the authors, few studies have been published for nickel based alloys. D. Wang et al. (9) have studied the electrochemical dissolution behavior on Inconel 718 at a current density of 1 A cm^{-2} in $NaNO_3$ solution and concluded that the dissolution begins through the pores of the anodic oxide film with a selective corrosion area and the formation of black products on the surface. On the other hand, P. Guo et al. (10) (11) have investigated the electrochemical behavior and the related anodic dissolution mechanism of the relieved – stress annealed laser solid formed (LSF) Inconel 718, which has a specific microstructure in comparison with the forged one (12). The electrochemical removal of the different phases of LSF Inconel 718 was explored through polarization tests, analysis of the microstructure and the surface products. The authors have shown that niobium element plays a leading role in the dissolution process. Indeed, they have observed that the Nb rich phase dissolves faster than the austenitic matrix because of the higher Nb electrode potential comparing to Ni. In addition, the oxidative process usually starts with the formation and the growth of an oxide film. Inside this film, the stoichiometry changes continuously in the first atomic layers at the interface film/oxide (13) (14). P. Novak et al. (15)

Mis en ligne le 3 janvier 2020 par Journal of Applied Electrochemistry
https://doi.org/10.1007/s10800-019-01386-z

have studied the influence of the presence of chlorate in the electrolyte on the anodic dissolution of various nickel alloys and they have concluded that no intergranular corrosion was observed in 15 wt.% $NaNO_3$ + 20 wt.% $NaClO_3$ electrolyte composition contrary to the usual bath of $NaNO_3$ 20 % wt. Moreover, Chun et al. (27) have reported that the nature of the anion is an important factor, allowing the production of a passivating oxide film. Thus, for (Fe-Ni) fin sheets, they observe that NO_3^- ions make it more difficult to change to the transpassive state than ClO_3- ions.

Thus, it appears that the dissolution mechanism of Inconel 718 is complex and sensitive to the electrolyte composition, the alloy content and its microstructure. Therefore, the purpose of this work is to improve the understanding of the forged Inconel 718 anodic dissolution behavior in different electrolytes. Thus comparative study of the relative electrochemical systems was performed, with the systematic analysis of the insoluble anodic products (IP), namely the so called black products, and the soluble dissolution products (SDP). Our main contribution in this paper concerns the positive impact of a new chelating agent use (sulfosalicylic acid SSA) in the electrolyte for the electrochemical dissolution of Inconel 718.

Specimen preparation and electrolytes

Rectangular specimens of 6 mm x 5 mm x 2 mm of Inconel 718 (Fe 17 wt.%, Cr 17 wt.%, Nb 5.6 wt %, Mo 3 wt.%, Al 0.4 wt.%, Ti 1.2 wt.%, Ni balance) were provided by Safran Aircraft Engines. The superalloy was fabricated by successive steps, Vacum Induction Melting (VIM), followed by Electro Slag Remelting (ESR) and finally by Vacum Arc Remelting (VAR). The samples were mechanically polished with successively finer grades of SiC papers up to 1200 and lastly with successive finer diamond suspension 3 µm and 1 µm in order to get a mirror-like aspect. They were finally rinsed with distilled water, degreased with acetone and dried with ethanol.

The synthesis of the individual phases γ'' and γ were carried out in a high frequency induction furnace under a controlled atmosphere of 500 mBar Ar and a voltage of 5kV. Precursors with purity between 99.5% and 99.95% were weighed for a 60 g load. The final composition of each phase was checked by at least 5 EDS-SEM analysis. Concerning the γ phase, post annealing treatment at 1200°C during 6h was necessary in order to obtain a homogeneous bulk sample. The chemical contents (% wt) of the individual phase γ was evaluated following: Al 0.3 ±0.1, Ti 1.1

Mis en ligne le 3 janvier 2020 par Journal of Applied Electrochemistry
https://doi.org/10.1007/s10800-019-01386-z

±0.1, Cr 17.4 ±0.2, Fe 17.7 ±0.4, Ni 53.4 ±0.4, Nb 5.5 ±0.2 and Mo 4.6 ±0.3. For the sake of simplification, the phase γ'' was fabricated with the Ni_3Nb composition as target instead of $Ni_{62}Nb_{18}Cr_7Fe_8\ Ti_2Mo_2$. Post annealing treatment was also necessary during 24h at 1250 °C in order to obtain a homogeneous sample. The sample was analyzed by SEM/EDS and the global composition was estimated according: Ni 74.9 ±0.3 (% wt) and Nb 24.9 ±0.3 (% wt).

Four electrolytes with different compositions were prepared from sodium nitrate (99 %, VWR product) and sodium chlorate (99 %, VWR product) and their compositions are given in Tab.1. The weight percentages of $NaNO_3$ and $NaClO_3$ are based from the literature data (9, 10) and they are a compromise between electrolyte resistance and machining precision. In particular, Da Silva et al. (26) have shown that electrolyte concentration influences greatly the accuracy of machining. In their work, higher accuracy is obtained with lower concentration. Nevertheless, by decreasing the ionic concentration of the bath increases the electrolyte resistance and the power consumption of the machining process.

Table 1 : Electrolytes composition and their corresponding measured electrical conductivity

Solution	Composition	Wt (%)	Molar concentration (mol L^{-1})	Electrical conductivity κ_{sol} (mS cm^{-1})
A	$NaNO_3$	8	0.94	65.1
B	$NaNO_3$	20	2.35	114
C	$NaNO_3$ + $NaClO_3$	15 + 20	1.76 + 1.187	136.5
D	$NaNO_3$ + sulfosalycilic acid (SSA)	20 + 2	2.35 + 0.1	122.1

Cyclic voltammetry and faradic efficiency measurement

Electrochemical investigations were carried out by cyclic voltammetry (CV) and anodic dissolution at fixed current density. Electrochemical studies were carried out using an Autolab 128 N potentiostat in a commercial glass cell from Ametek (model K0235) in vertical configuration with the Inconel plates as working electrode (WE). A platinum grid and a saturated Ag/AgCl electrode were used respectively as counter electrode (CE) and reference

Mis en ligne le 3 janvier 2020 par Journal of Applied Electrochemistry
https://doi.org/10.1007/s10800-019-01386-z

electrode. All the potentials are expressed throughout this work respect to the reference electrode. The inter-electrode WE-CE distance was 9 cm.

The anodic dissolution behavior of Inconel 718 was studied in each electrolyte at room temperature. Each electrochemical parameter set was repeated at least three times. Cyclic voltametries were performed between -0.3 V (Ag/AgCl/Sat. KCl) and 1.5 V (Ag/AgCl/Sat. KCl) with a scan rate of 10 mV/s. Moreover, dissolutions were achieved by chronopotentiometry (CP) at a fixed anodic current density of 1.025 A cm^{-2}. The active surface area was equal to 0.78 cm^{-2}.

The determination of the faradic efficiency was based on weight-loss measurements, described as follows. The theoretical weight loss ΔW_{theo} was calculated by considering the oxidation of each element *i* of the superalloy and taking account their specific valence z_i, their Molar Mass M_i and their mass percent w_i according the following equation (9, 25) :

$$\Delta Wtheo = I \times t \times \sum_{i=1}^{n} \left(\frac{w_i}{100}\right) \times \frac{M_i}{z_i \times F} \qquad (1)$$

With I the applied current (A), t the duration of the oxidation (s), and F the Faraday constant (96 485 A s mol^{-1}). All the anodic dissolutions were performed at a fixed applied coulometric charge of 3288 C, corresponding to a theoretical dissolved mass of 1g for pure nickel. The faradic efficiency η was defined as:

$$\eta = \frac{\Delta Wexp}{\Delta Wtheo} \qquad (2)$$

where ΔW_{exp} was the experimental weight loss after the surface cleaning step. The latter consist on the removing of insoluble anodic products (IP) in a 15 wt.% HCl solution assisted with ultrasound during 3 minutes (16).

Characterizations

X-ray diffraction (XRD) and Scanning Electron Microscopy (SEM)completed with Dispersive Energy Spectrometry (EDS) were used to characterize the insoluble anodic products (IP), whereas the tested electrolyte was analyzed by inductively coupled plasma (ICP) in order to determine dissolved elements concentration.

Mis en ligne le 3 janvier 2020 par Journal of Applied Electrochemistry
https://doi.org/10.1007/s10800-019-01386-z

The microstructure, of the Inconel 718 phases and the anodic solid products were characterized using Scanning Electron Microscope (SEM) (Tescan Vega 3) at 30 kV accelerating voltage. The elemental analysis was done by Energy Dispersive X-ray Spectroscopy (EDS) from detector attached to the SEM (Nano,Bruker).

Following the anodic dissolution experiments, the electrolytes, including Insoluble anodic Products (IP), were acidified to pH 1 with pure nitric acid in order to solubilize the produced metallic hydroxides and then filtered them. The content of the dissolved metals was measured by means of ICP-AES (Inductively Coupled Plasma Atomic Emission Spectrometry, Ultima Jobin Yvon) machine. For each element, the result obtained is the average of two different wavelengths. The residual solids were successively rinsed, dried and then analyzed by X-ray diffraction (XRD) using a Bragg-Brentano theta-theta diffractometer (Bruker, D8 advance) equipped with a copper anode of wavelength λ (Kα) = 1.5406 Å. The patterns were realized with 2Θ values ranging from 10° to 110°. Cross-section visualizations of the anodic films were analyzed by SEM. For this purpose, the samples were metallized by a sputtered gold layer in order to improve the electrical conductivity of the anodic films. A final protective nickel was then electroplated on the substrate. The samples were subsequently cut, hot coated and then polished.

Results and discussion

Electrochemical study

Typical CV and the corresponding Tafel plots are given in Fig1.a and Fig.1.b. A passive region, with no active dissolution, was observed in the range from OCP to about 1.1 V (Ag/AgCl/Sat. KCl), resulting from a formation of an oxide layer (Fig. 1.a). It has been reported that the main passivation product on nickel surface is the cubic NiO phase, with the possible formation of Ni_2O_3 phase (17) .For Ni-Cr alloys, it has been reported that $Ni(OH)_2$ is formed, at low potentials, and it is transformed into NiO when the potential increases (18). Anodic potential sweeps were performed up to 1.5 V (Ag/AgCl/Sat. KCl). Anodic dissolution takes place in transpassive potential region after the destruction of the protective passive film formed on the anode surface. The mechanism of the transpassivation is very complex and many anodic reactions are occurring during high rate dissolution. Table 2 illustrates the possible anodic reactions of the major elements of Inconel 718 and their associated standards potentials.

Mis en ligne le 3 janvier 2020 par Journal of Applied Electrochemistry
https://doi.org/10.1007/s10800-019-01386-z

Tab 2 : Possible anodic reactions of the major elements of Inconel 718 and their related standard potentials versus the standard hydrogen electrode (SHE) (11)

Element	Reaction	Standard potentials (V (SHE))
Ni	$Ni \rightarrow Ni^{2+} + 2e^-$	-0.25
Fe	$Fe \rightarrow Fe^{2+} + 2\ e^-$	-0.44
Cr	$Cr \rightarrow Cr^{3+} + 3\ e^-$	-0.74
Nb	$2Nb + 5H_2O \rightarrow Nb_2O_5 + 10H^+ + 10\ e^-$	-0.60
Mo	$Mo \rightarrow Mo^{3+} + 3\ e^-$	-0.2
Al	$Al \rightarrow Al^{3+} + 3\ e^-$	-1.66
Ti	$Ti + 2H_2O \rightarrow TiO_2 + 4H^+ + 4\ e^-$	-0.86

From the literature data, the transpassive dissolution of nickel in nitrate solution is initiated by a local breakdown of the passive film, in a similar way to the pitting behavior of passive metals in aggressive media under corrosion conditions (19). Two possible pathways in the transpassive state have been proposed by I. Betova et al.. (20), namely the oxidative dissolution and the anion-assisted solubilisation. It has been suggested that, at high potentials, an interaction between nickel cations and solutions anions in the interface film/electrolyte leads to the formation of surface intermediate species.

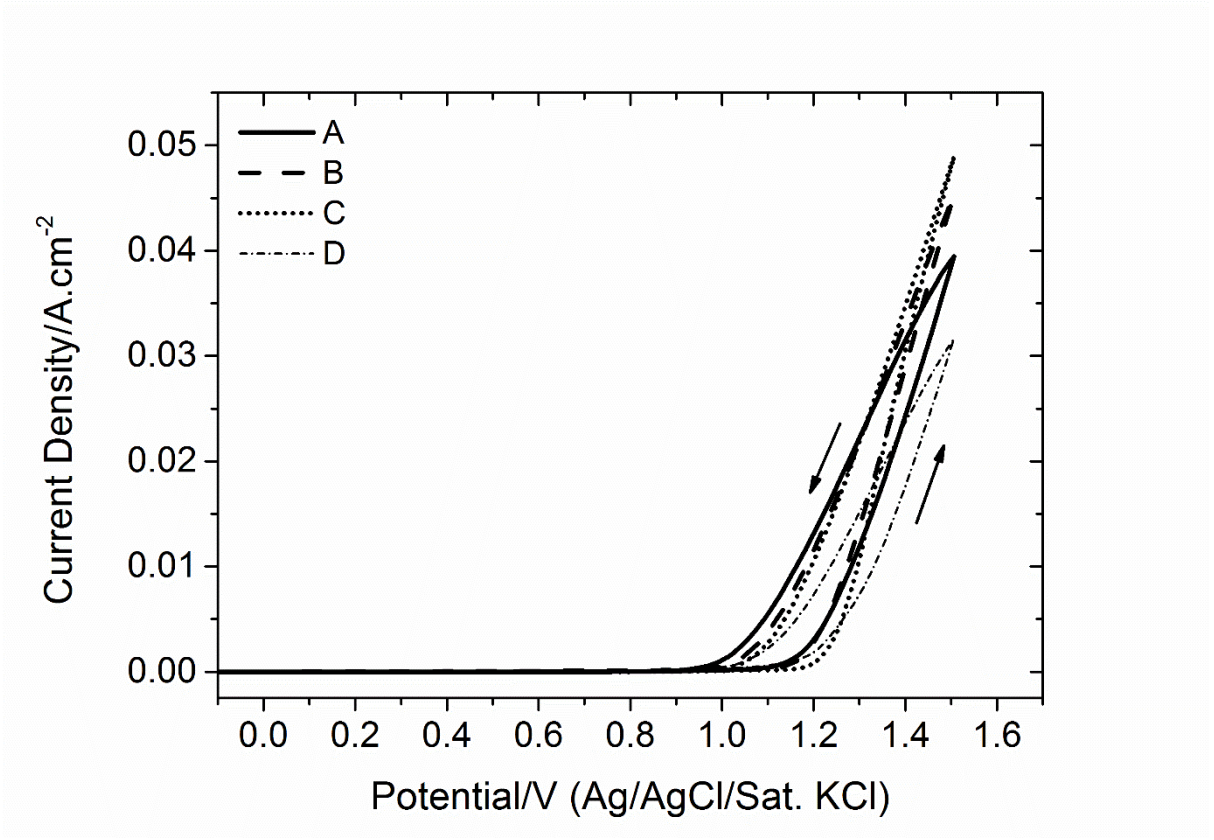

Fig. 1.a : Potentiodynamic current vs potential curves of Inconel 718 in solutions A, B, C and D. Scanning rate 10 mV s^{-1}

Mis en ligne le 3 janvier 2020 par Journal of Applied Electrochemistry
https://doi.org/10.1007/s10800-019-01386-z

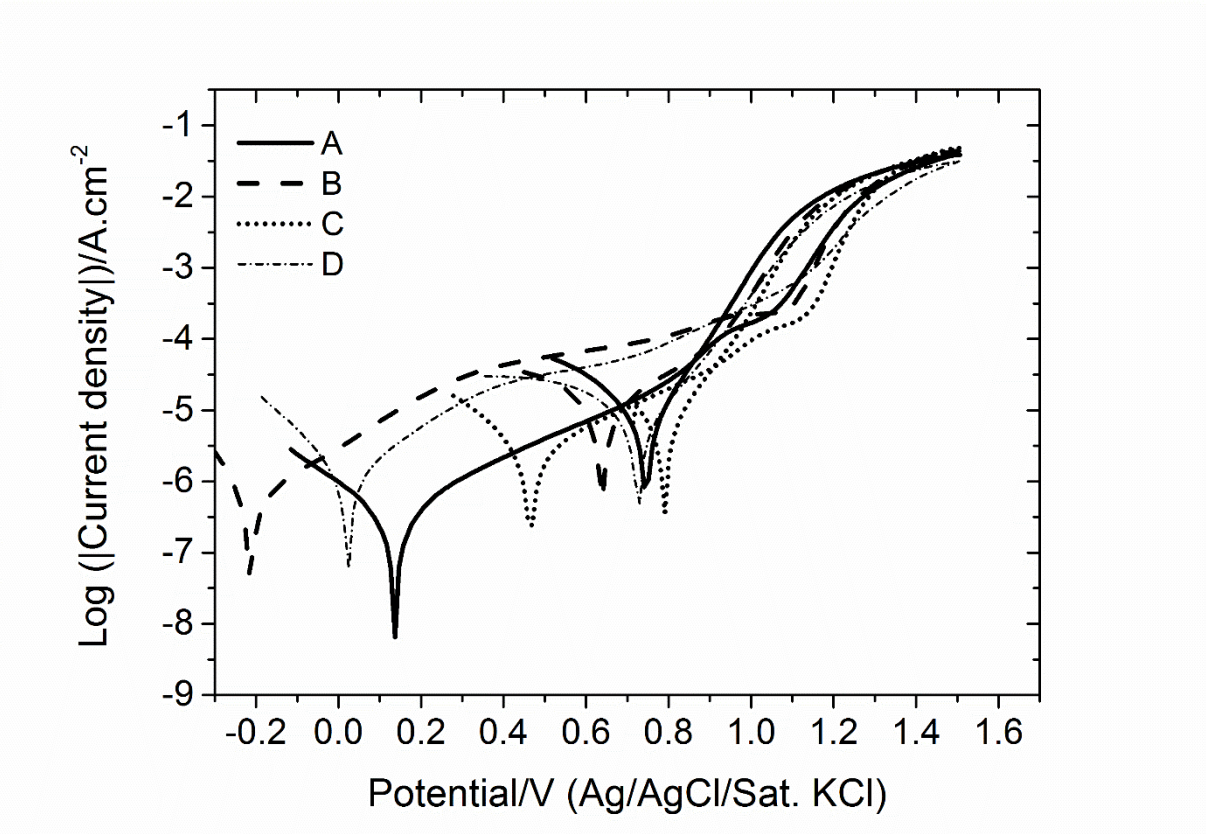

Fig. 1.b: Corresponding Tafel plot of Inconel 718 in solutions A, B, C and D. Scanning rate 10 mV s^{-1}

From these data, we have systematically determined the voltage ΔE, the difference between the corrosion potential E_{corr} and the dissolution potential E_d (Fig. 2). Indeed from a study of electrochemical dissolution of cast iron in $NaNO_3$ (21), the authors have demonstrated the influence of ΔE on the efficiency of the anodic dissolution. The E_d was arbitrary chosen for a current density 0.002 A cm^{-2}, whereas the E_{corr}. was obtained from the Tafel plot. For the solution A, the ΔE value is the about 1.05 V) whereas the corresponding values for the solutions B and D are lower and close to each other. The lowest ΔE value is obtained for the mixture 15% $NaNO_3$ + 20 % $NaClO_3$ and does not exceed 1 V. This observation is probably due to the formation of Chloride anions resulting to the decomposition of the chlorate anions according to the reaction (1) (22):

$$3\ Ni + ClO_3^- + 6\ H^+ \rightarrow 3Ni^{2+} + Cl^- + 3\ H_2O \quad \text{Equation (1)}$$

It can be stated that the presence of Cl^- ions disturbs the stability of the native oxide layer and leads to an earlier potential appearance of the transpassive region. This behavior presents some analogy to well-known film breakdown phenomena in chloride solutions leading to pitting (19).

Mis en ligne le 3 janvier 2020 par Journal of Applied Electrochemistry
https://doi.org/10.1007/s10800-019-01386-z

Assuming that the relationship between the current density and the potential is based on the Ohm's law in the transpassive region (8) (9), the effective resistance R_{eff} was systematically calculated from the reciprocal of slopes j=f(E) in the forward direction (Fig. 3a). Several contributions are involved in this term R_{eff}: the electrolyte resistance, the oxide film resistance formed on the surface as well as the charge transfer. The R_{eff} data are practically halved for the solution B, C and D by comparison with the solution A. Thus it appears that the values of R_{eff} have roughly the same inverse trend than with those of the electrical ionic conductivity σ of the corresponding electrolyte. In order to get a finer interpretation of the main contribution of the effective resistance, R_{eff} was plotted versus the inverse of the electrolyte conductivity in the Figure 3b. A linear fit is obtained with a slope close to 1 suggesting that the effective resistance is mainly influenced by the bath electrical conductivity.

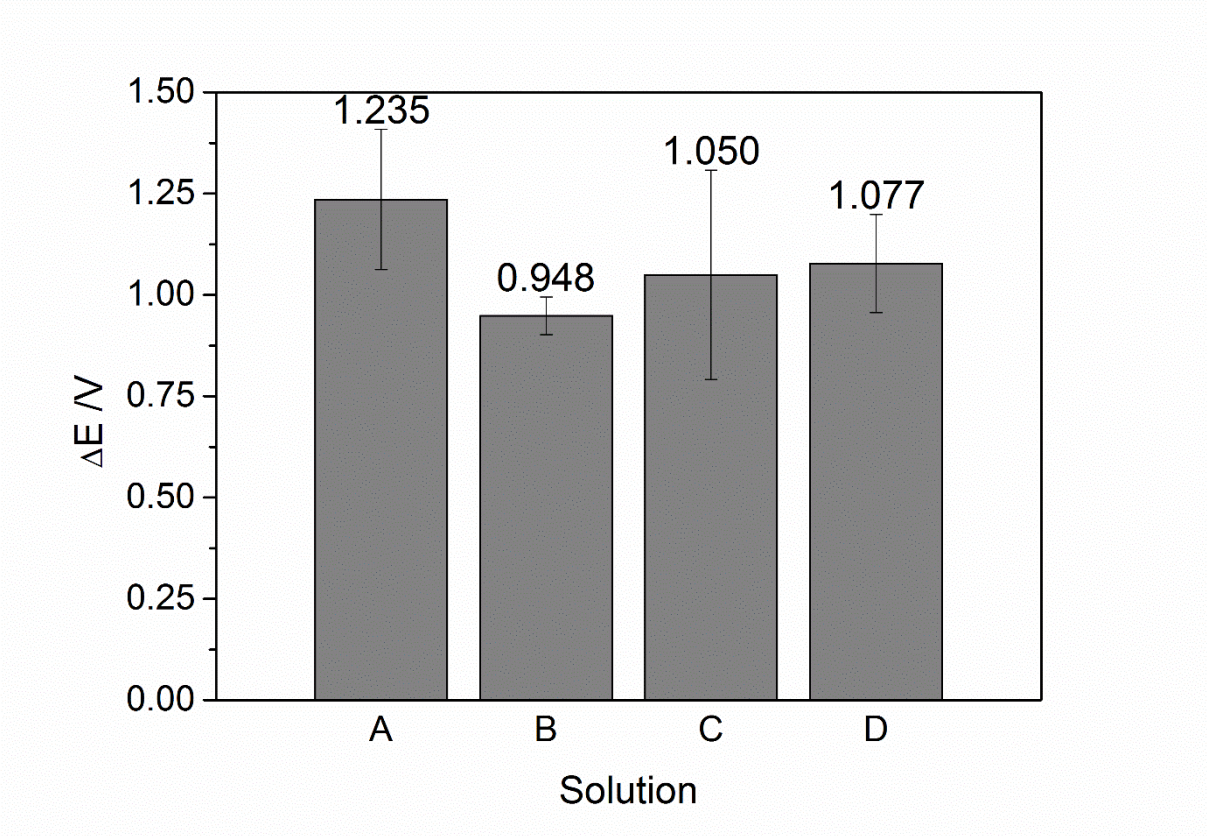

Fig. 2: ΔE as a function of the different tested electrolytes

Mis en ligne le 3 janvier 2020 par Journal of Applied Electrochemistry
https://doi.org/10.1007/s10800-019-01386-z

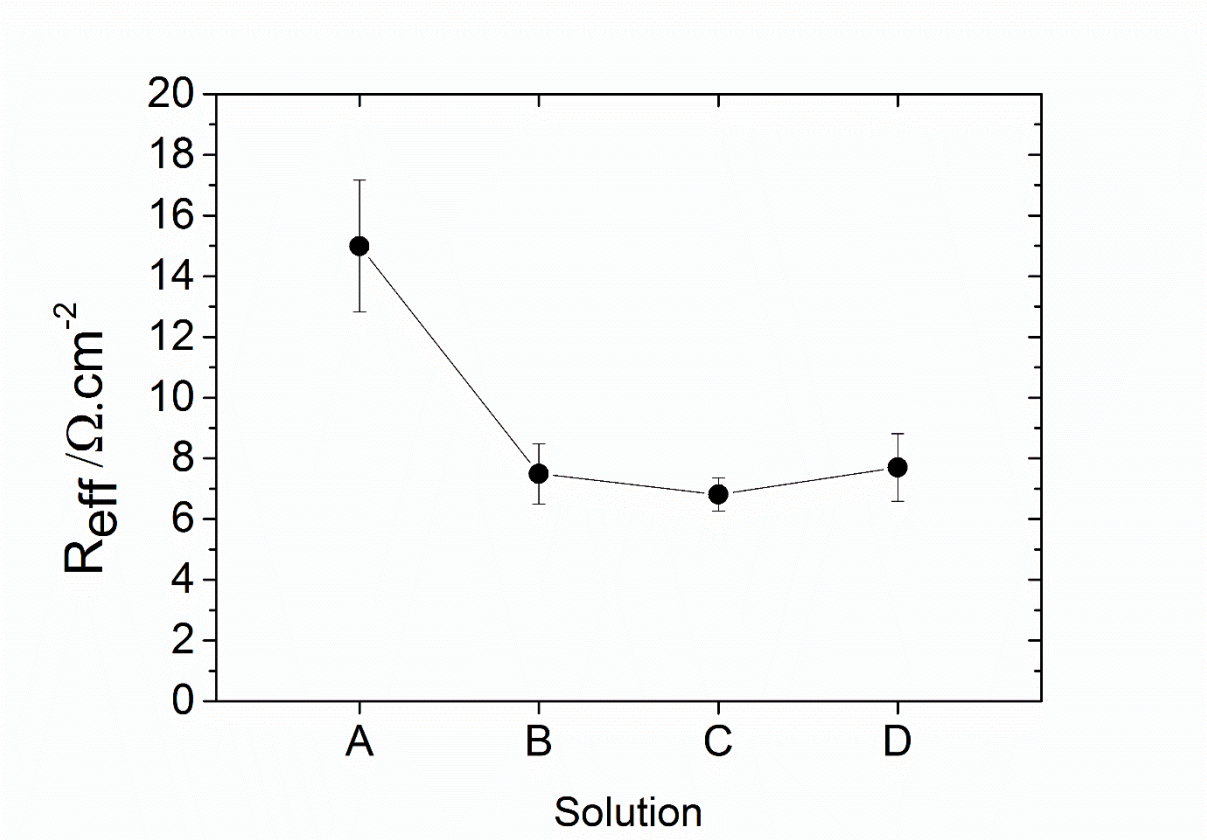

Fig. 3.a: R_{eff} as a function of the different tested electrolytes

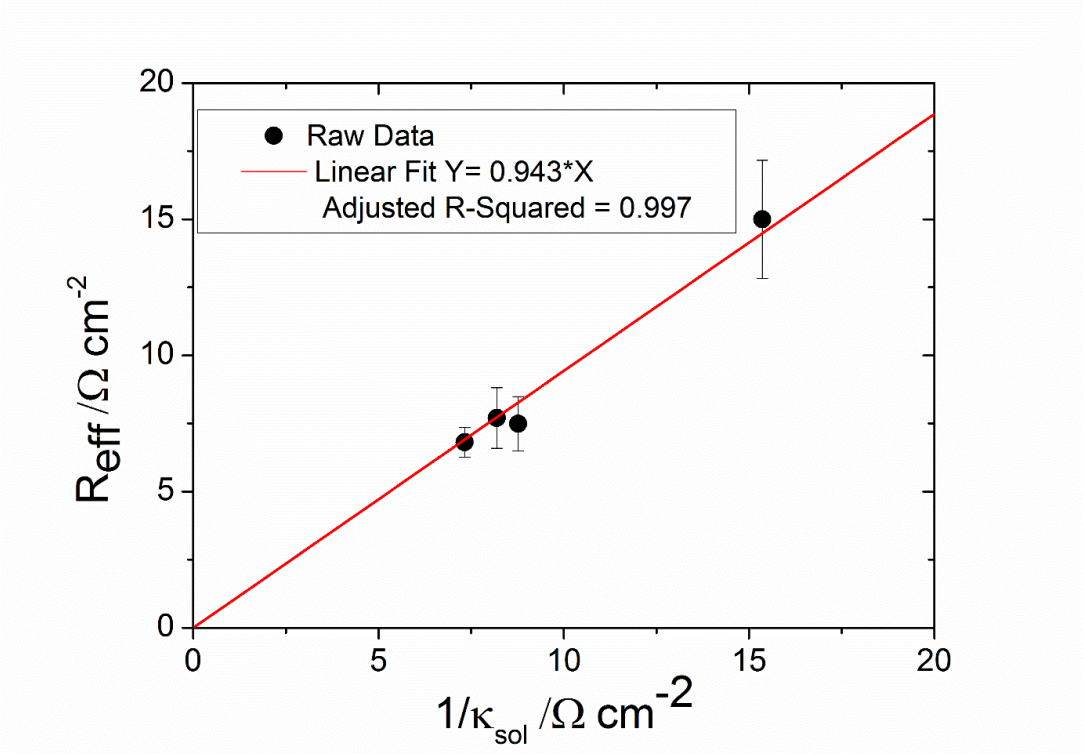

Fig. 3.b: linear relationship between R_{eff} and $1/\kappa_{sol}$ for the different tested electrolytes

Mis en ligne le 3 janvier 2020 par Journal of Applied Electrochemistry
https://doi.org/10.1007/s10800-019-01386-z

Faradic efficiency

Weight loss was systematically measured for each electrolyte and the faradic efficiency values were calculated by equation (2) and tabulated in Tab 3 :

Tab 3 : Faradic efficiencies calculated for each electrolyte

Solution	Current efficiency (%)
A	76.76 ± 0.4
B	75.85 ± 0.4
C	79.38 ± 0.6
D	76.99 ± 0.1

The presence of chlorate ions in the bath (solution C) leads to slightly higher current efficiency of Inconel 718 in comparison with solutions A, B and D. M. Datta et al..(23) have reported that this higher faradic efficiency is due to the chlorate reduction at active sites on the anode following the corrosion reaction according to equation (1).

Inconel 718 microstructure

Fig.4a displays the microstructure of the forged Inconel 718 with the austenitic matrix (MP) rich of Ni, Fe, and Cr. intergranular precipitates are so called secondary phase (SP), mainly made of Ni and Nb. Fig.4.b illustrates the basic components (wt %) of the MP and SP phases. The microstructure of Inconel 718 includes also carbonitride titanium (C1) and niobium carbides (C2). The EDS results of C1 and C2 are listed in Fig.4. c and d respectively, showing that the contents of Nb and Ti are higher than ones in the phases MP and SP.

Mis en ligne le 3 janvier 2020 par Journal of Applied Electrochemistry
https://doi.org/10.1007/s10800-019-01386-z

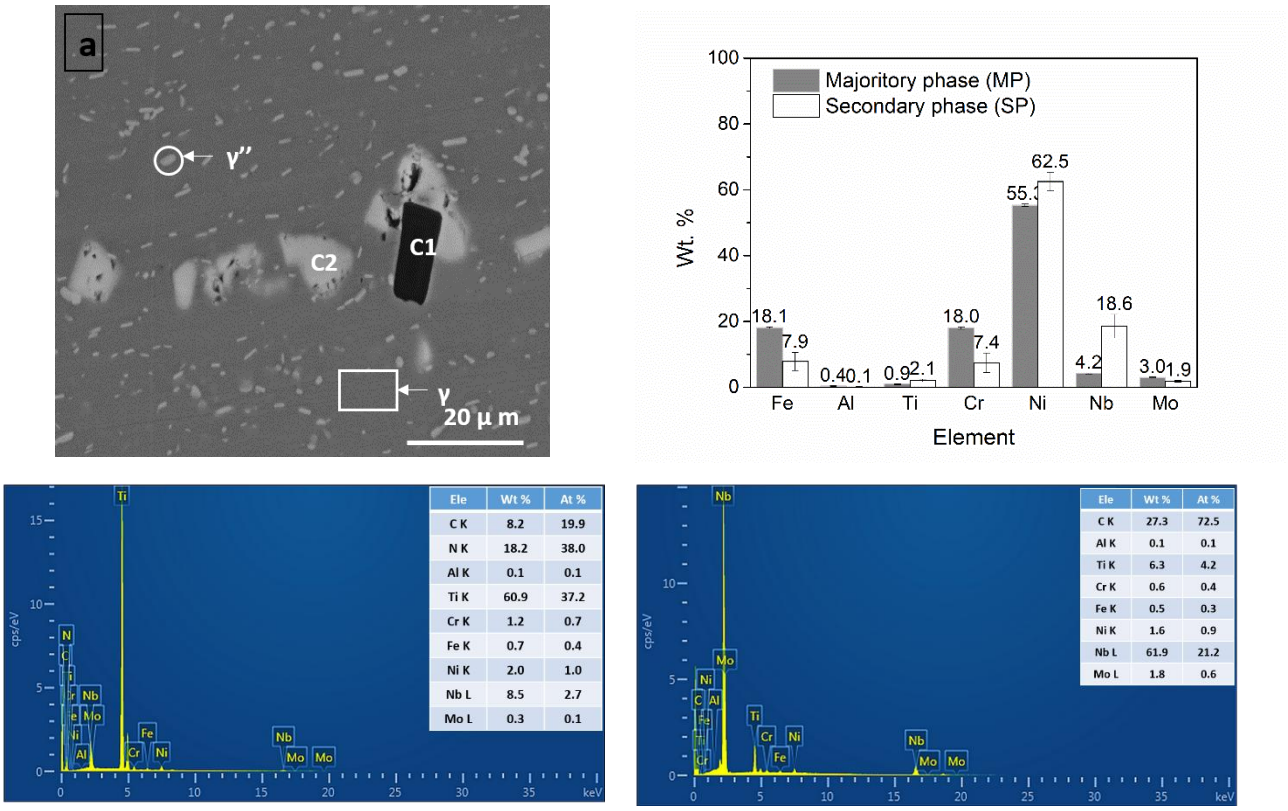

Fig. 4 : a/ SEM surface image of polished Inconel 718, b/Histograms of the MP and SP phase compositions, c/EDS spectrum and related chemical compositions of the C2 carbides , and of the C1 one d/.

Analysis of the anodic dissolution products

Following the dissolution process, the insoluble anodic products were collected from the used electrolyte and were identified by XRD and compared with the initial Inconel 718 substrate. Fig. 5. shows the resulting diffraction patterns in the four electrolytes. The pattern of the Inconel 718 corresponds to the austenitic structure Ni-Cr-Fe space group Fm-3m (JCPDS n°33 -0397) with adjusted cell parameters from 3.591 Å to 3.597 Å. This difference of lattice parameter can be explained by the difference of the chemical composition between the experimental pattern and the database pattern. The most intense diffraction peak of the tetragonal Ni_3Nb structure (space group I4/mmm) (COD n°1521755) can also be detected corresponding to the secondary phase SP. The patterns of the insoluble products (IP) obtained with the different electrolytes, are mainly identical and correspond to the precipitates Ni_3Nb under different phases: the orthorhombic δ phase Pmmn ((COD n°1522733) and the tetragonal γ'' phase space group I4/mmm (COD n° 1521755). The hexagonal $Ni_{0.75}Nb_{0.125}Ti_{0.125}$ phase space group P63/mmc (COD n°1522732) was also found.

Mis en ligne le 3 janvier 2020 par Journal of Applied Electrochemistry
https://doi.org/10.1007/s10800-019-01386-z

Thus this analysis shows that crystallized insoluble anodic products are mainly composed of the γ'' phase, coming from a potential debonding mechanism from the surface of the alloy during the electrochemical dissolution process (11).

Mis en ligne le 3 janvier 2020 par Journal of Applied Electrochemistry
https://doi.org/10.1007/s10800-019-01386-z

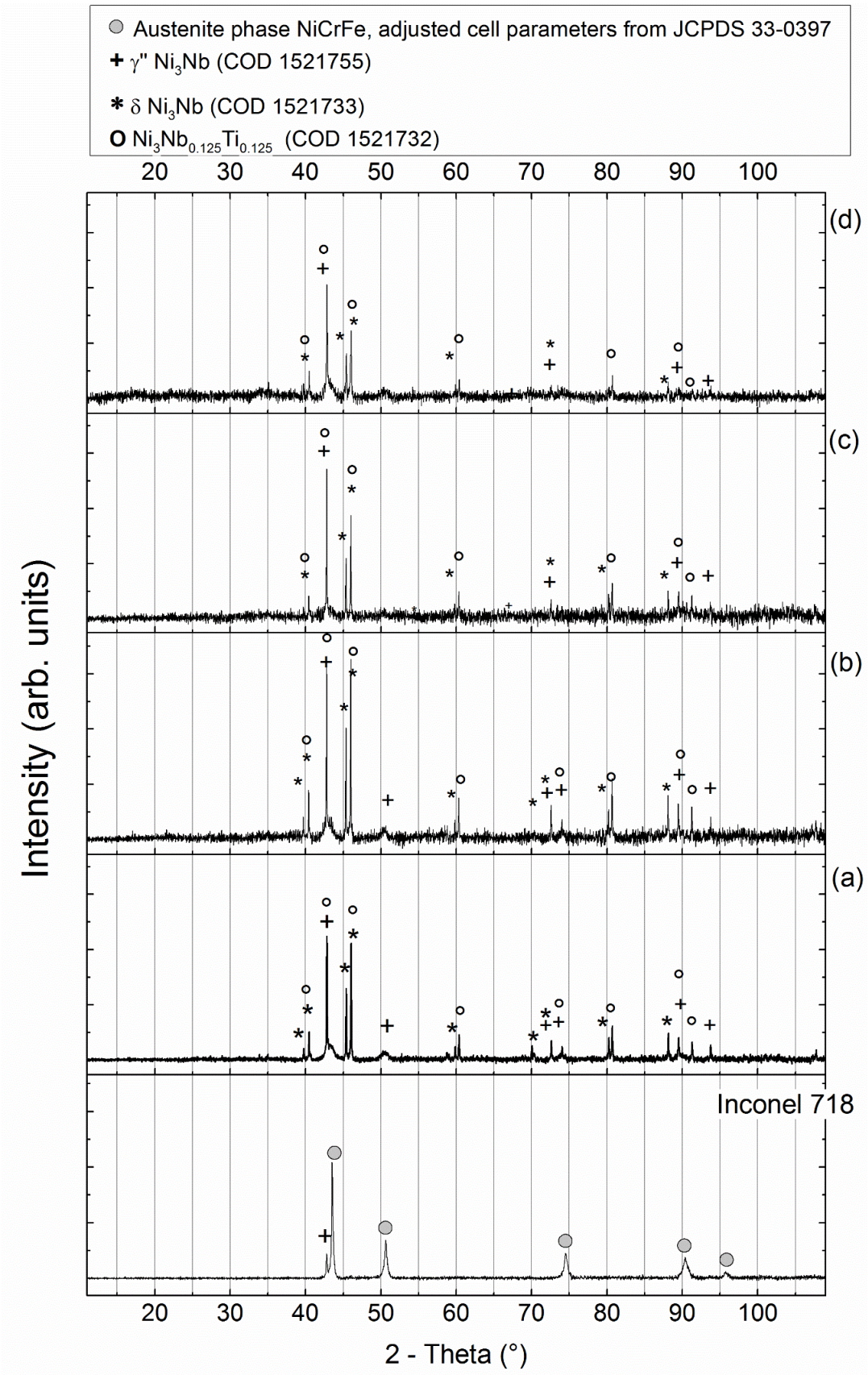

Fig. 5: Diffraction patterns of the Inconel 718 and IP obtained after anodic dissolution process in solutions: (a) A, (b) B, (c) C and (d) D

Mis en ligne le 3 janvier 2020 par Journal of Applied Electrochemistry
https://doi.org/10.1007/s10800-019-01386-z

In order to investigate further the above hypothesis, surface resulting from dissolution was studied by SEM/EDS cross-section views. Fig. 6 shows that the substrate (Inconel 718) is covered by a surface layer of anodic products. Indeed a porous structure of oxide film was adopted (9), and particles with the same shape and size as the γ'' ones were identified. Regardless the kind of electrolyte, the Ni_3Nb phase was located in the surface products and seems to be confined into an oxide phase (white particles) as shown in Fig. 6. However, in the solution D, the oxide layer thickness on the surface has considerably decreased. This can be explained by the chelating action of the SSA reagent, leaching the main elements and thereby decreasing their proportion on the surface. Moreover, the anodic layer seems to be more compact in presence of chlorates (solution C), but with no passivation effect as previously suggested by the effective resistance R_{eff}. With such large differences of the layer morphologies, these results confirm that the effective resistance is mainly governed by the electrolyte resistance and not by the oxide resistance.

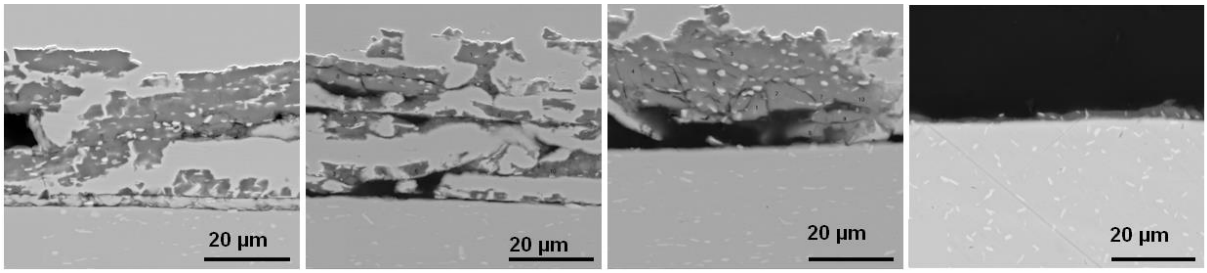

Fig. 6: SEM images of cross-view sections of Inconel 718 after electrochemical dissolution in solutions a/ A, b/ B, c/ C and d/D

Mis en ligne le 3 janvier 2020 par Journal of Applied Electrochemistry
https://doi.org/10.1007/s10800-019-01386-z

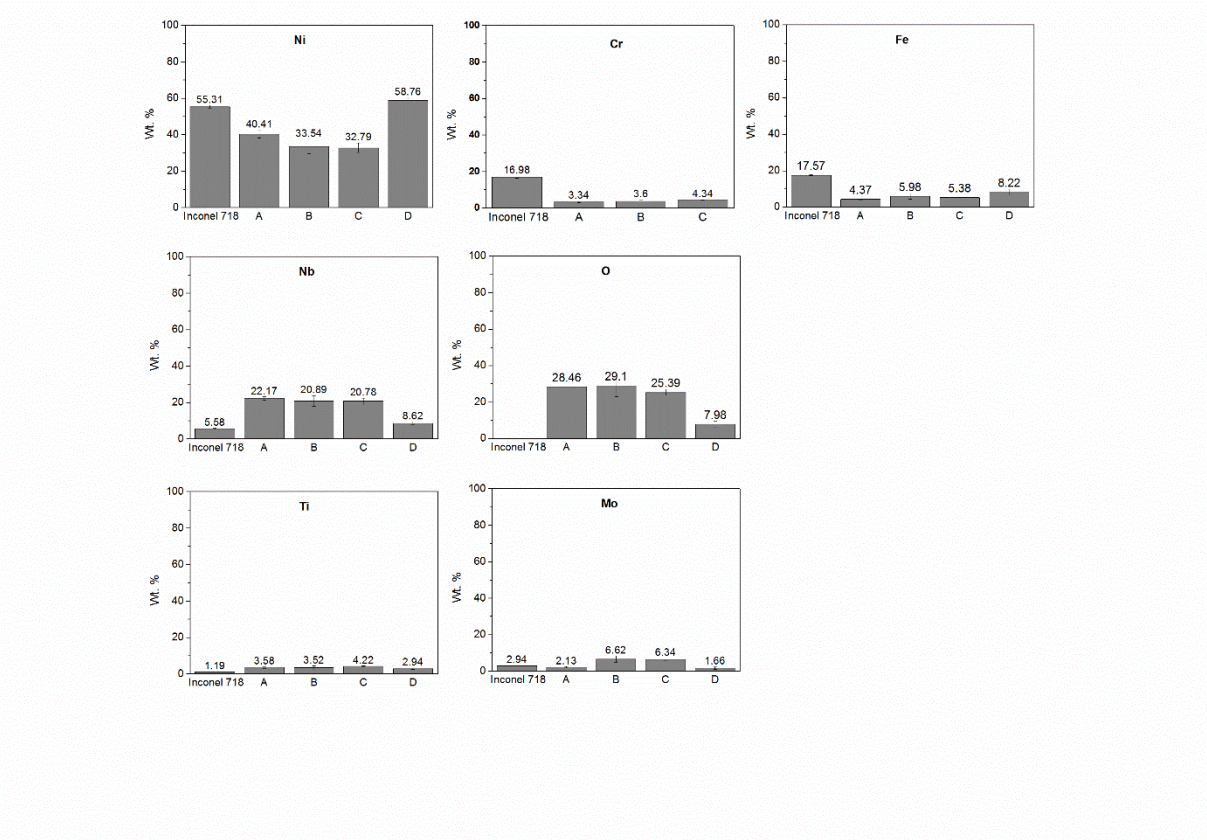

Fig. 7: SEM analysis of Inconel 718 after electrochemical dissolution in a/ A, b/ B, c/ C and d/D

The histograms of Fig. 7 represent the weight contents of the elements in the Inconel 718 and in the surface layer obtained after anodization in different electrolytes. A depletion of Cr and Fe is observed compared to the initial composition of the Inconel 718 in solution A, B, and C. On the contrary, a clear enrichment of Nb, Mo and Ti is noticed. This enrichment is accompanied by the oxygen increasing content, due to the potential presence of oxide, such as Ni, Nb and Ti oxides. From the literature data (11), the Nb content is explained by the presence of γ'' particles and Nb oxides (Nb_2O_5), since niobium is insoluble in aqueous phase. In the electrolyte D, the results evidence an increase Ni and Cr content and a decrease of Nb, Ti, Mo and O content. It is concluded that the elements Nb, Mo and Ti are oxidized and probably solubilized through the formation of dissolved complexes, by the presence of sulfosalycilic acid as a chelating reagent. This hypothesis will be validated by the chemical analysis of the electrolytes.

Analysis of the used electrolytes after anodization

Table 4 collects the result of ICP analysis of the different used electrolytes. The data, expressed as relative percentages by weight, are compared with the global chemical composition of the

Mis en ligne le 3 janvier 2020 par Journal of Applied Electrochemistry
https://doi.org/10.1007/s10800-019-01386-z

Inconel 718. For the solutions A, B and C, it is obvious to notice that the elements Fe, Ni and Cr are preferentially dissolved, while the contents of Ti, Mo, Al and Nb are depressed. Those results are in good agreement with the previous SEM/EDS analysis, suggesting that Ti, Mo, Al and Nb of the matrix have turned into oxides.

Tab 4 : ICP-AES analysis of used electrolytes

solution	Mo		Cr		Ni		Al		Fe		Ti		Nb	
	ppm	% wt.	ppm	% wt.	ppm	% wt.	ppm	% wt.	ppm	% wt.	ppm	% wt.	ppm	% wt.
A	38.4 ± 0.7	1.46	553 ± 5	21.09	1510 ± 33	57.58	7.90	0.30	511± 5.5	19.49	2.2 ± 0.15	0.08	*	*
B	9.9 ± 0.5	0.39	534 ± 12	21.14	1465 ± 23	58.00	6.60	0.26	508 ± 9	20.11	2.2 ± 0.03	0.09	*	*
C	6.8 ± 0.3	0.32	472 ± 12	21.87	1339 ± 4	62.05	6.00	0.28	332 ± 2.5	15.39	2.0 ± 0.04	0.09	*	*
D	63.1 ± 2.3	6.22	387 ± 7	38.15	358 ±	35.30	4.20	0.41	143.3 ± 1	14.13	3.8 ± 0.1	0.37	17.1± 0.1	1.69
Inconel 718		***2,0***		***17.00***		***55,3***		***0,4***		***17,6***		***1,2***		***5,6***

*Below the detection threshold

In presence of sulfosalicylic acid, the contents of Mo, Ti and Nb have considerably increased in relative proportions. Concerning the element Niobium, this result can be explained by the chelating capacity of sulfosalicylic acid with NbO^{3+} (log Kf = 4.0) (24). Similar comment can be made for the element Al, for which an increase of its dissolved concentration is also observed in presence of SSA. This behavior can be similarly explained by the chelating properties of sulfosalicylic acid with Al^{3+} (log Kf = 12.9) (24). Surprisingly, the concentrations of the main elements of the matrix γ have decreased in the electrolyte D, although sulfosalicylic acid is a chelating agent of Ni^{2+} (log Kf = 10.2), Fe^{3+} (log Kf =10) and Cr^{3+} (log Kf = 9.6) (24).

In order to have a better understanding of the influence of the chemical reagent SSA on the anodic dissolution, experiments were performed on the two main phases of Inconel 718. The faradic efficiencies for the phases γ'' and γ are compared with and without SSA in the table 4.

Mis en ligne le 3 janvier 2020 par Journal of Applied Electrochemistry
https://doi.org/10.1007/s10800-019-01386-z

Tab 5 : Comparison of the faradic efficiencies (%) of the individual phases of the Inconel 718 without SSA (solution A) and with SSA (Solution D)

	Solution B	Solution D
phase γ''	79.7 ± 1.3	65.6 ± 3.2
phase γ	63.5 ± 0.7	69.3 ± 0.8

The results show that the phases γ'' and γ behave differently. Thus the phase γ'', namely Ni_3Nb, has a lower anodic efficiency in presence of SSA, whereas the austenitic phase γ exhibits a better faradic efficiency. By taking into account the previous ICP analysis, it appears that the higher amounts of the dissolved metallic contents of Mo, Ti and Nb come from the better dissolution of the phase γ rather than the γ'' one. Surprisingly the chelating properties of the solution D with the Niobium seems to be more efficient for the phase γ, in probable connection with their specific microstructure. Whatever, the improvement of the anodic dissolution of the Inconel 718 in presence of sulfosalicylic acid appears to be due to the enhanced dissolution of its matrix.

Conclusions

This paper has focused on the electrochemical dissolution behavior of Inconel 718 in pure $NaNO_3$ solutions and in the mixed electrolytes (15 wt.% $NaNO_3$ + 20 wt.% $NaClO_3$ and in 20 wt.% $NaNO_3$ + 2.4 % wt SSA). Based on the electrochemical study of the anodic behavior, the microstructure analysis of the anodic surface products and the dissolved elements in the four tested electrolytes, the mains results are the following ones:

- Whatever the electrolyte composition, the anodic dissolution mechanism corresponds to the heaving of the particles of the γ" phase from the surface layer to the electrolyte. In parallel, the observed anodic film is mainly made of Nb and Ti oxides.
- The presence of chlorates ions, leads to a depressed energy required to start electrochemical dissolution and to improve current efficiency, with an accelerated corrosion process. Moreover, a thicker oxide layer is observed with no passivation effect.
- In presence of sulfosalicylic acid, the amount of dissolution products remaining on the sample surface decrease considerably and niobium is dissolved into the aqueous phase. Therefore, it can be concluded that sulfosalicylic acid through its chelating property has a beneficial effect for an improved anodic dissolution process of Inconel 718

Mis en ligne le 3 janvier 2020 par Journal of Applied Electrochemistry
https://doi.org/10.1007/s10800-019-01386-z

References

1. D. Dudzinski, A. Devillez, A. Moufki, D. Larrouquère, V. Zerrouki, V. Vigneau. A review of developments towards dry and high speed machining of Inconel 718 alloy. Int J Mach Tools Manuf. 2004;44:439‑56.

2. M. Burger, KL. oll, E. A. Werner, A. Platz. Electrochemical machining characteristics and resulting surface quality of the nickel-base single-crystalline material LEK94. J Manuf Process. 2012;14:62‑70.

3. M.Schneider, N.Schubert, S.Höhn, A.Michaelis. Anodic dissolution behaviour and surface texture development of cobalt under electrochemical machining conditions. Electrochim. Acta. 2013;106:279– 287.

4. C. Rosenkranz, M.M. Lohrengel, J.W. Schultze. The surface structure during pulsed ECM of iron in NaNO3. Electrochim. Acta. 2009;50:2009–2016.

5. J. Bannard. Effect of flow on the dissolution efficiency of mild steel during ECM. J Appl Electrochem. 1977;7:267‑70.

6. M.M. Lohrengel, I. Kluppel, C. Rosenkranz, H. Bettermann, J.W. Schultze. Microscopic investigations of electrochemical machining of Fe in NaNO3. Electrochim. Acta. 2003;48:3203‑11.

7. L. Tang, B. Li, S. Yang, Q. Duan, B. Kang. The effect of electrolyte current density on the electrochemical machining S-03 material. Int J Adv Manuf Technol. 2014;71:1825–1833.

8. T. Haisch a, E. Mittemeijer, J.W. Schultze. Electrochemical machining of the steel 100Cr6 in aqueous NaCl and NaNO3 solutions: microstructure of surface films formed by carbides. Electrochim. Acta. 2001;47:235–241.

9. D. Wang, Z. Zhu, N. Wang, D. Zhu, H. Wang. Investigation of the electrochemical dissolution behavior of Inconel 718 and 304 stainless steel at low current density in NaNO3 solution. Electrochim. Acta. 2015;156:301‑7.

10. G. Pengfei, L. Xin, J. Li, Y. Zhang, M. Song, W. Huang. Electrochemical behavior of Inconel 718 fabricated by laser solid forming on different sections. Corros. Sci. 2017;79‑89.

11. P. Guo, X. Lin, J. Xu, J. Li, J. Liu, W. Huang. Electrochemical Removal of Different Phases from Laser Solid Formed Inconel 718. J Electrochem Soc. 2017;164:E151‑7.

12. T. Trosch, J. Strößner, R. Stefec, U. Glatzel. Microstructure and mechanical properties of selective laser melted Inconel 718 compared to forging and casting. Mater Lett. 2016;164:428‑31.

13. M. Bojinov, I. Betova, G. Fabricius, T. Laitinena, R. Raiche, T. Saario. The stability of the passive state of iron - chromium alloys in sulphuric acid solution. Corros. Sci. 1991;41:0446‑73.

14. I. Betova, M. Bojinov, P. Kinnunen, T. Laitinen, P. Pohjanne, T. Saario. Mechanism of transpassive dissolution of nickel-based alloys studied by impedance spectroscopy and rotating ring-disc voltammetry. Electrochim. Acta. 2002;47:2093‑107.

15. P. Novak, I. Rousar, R. Stefec, V. Cihal. Intergranular Corrosion in Electrochemical Machining. Mater Chem Phys. 1984;10:155‑61.

Mis en ligne le 3 janvier 2020 par Journal of Applied Electrochemistry
https://doi.org/10.1007/s10800-019-01386-z

16. NF EN ISO 8407. In.

17. T. Tzvetkoff, P. Gencheva. Mechanism of formation of corrosion layers on nickel and nickel-based alloys in melts containing oxyanions—a review. Mater Chem Phys. 2003;82(897–904).

18. M. Bojinov, G. Fabricius, P. Kinnunen, T. Laitinen, K. Ma¨kela, T. Saario, et al.. The mechanism of transpassive dissolution of Ni–Cr alloys in sulphate solutions. Electrochim. Acta. 2000;45:2791–2802.

19. M. Datta, D. Landolt. Film breakdown on nickel under transpassive dissolution conditions in sodium nitrate solutions. J Electrochem Soc. 1977;124(4):483‑9.

20. I. Betova, M. Bojinov, T. Tzvetkoff. Oxidative dissolution and anion-assisted solubilisation in the transpassive state of nickel–chromium alloys. Electrochim. Acta. 2004;49:2295–2306.

21. O. Weber, M. Weinmann, H. Natter, D. Bähre. Electrochemical dissolution of cast iron in NaNO3 electrolyte. J Appl Electrochem. 2015;45:591‑609.

22. M. Datta, D.Landolt. On the role of mass transport in high rate dissolution of iron and nickel in ECM electrolytes—I. Chloride solutions. Electrochim. Acta. 1980;25:1255‑62.

23. M. Datta, D.Landolt. On the role of mass transport in high rate dissolution of iron and nickel in ECM electrolytes—II. Chlorate and nitrate solutions. Electrochim. Acta. 1980;25:1255‑62.

24. A. Ringbom. Les complexes en chimie analytique. Dunod; Paris 1967.

25. Klocke, F.; Zeis, M.; Klink, A.; Veselovac, D., Experimental Research on the Electrochemical Machining of Modern Titanium- and Nickel-based Alloys for Aero Engine Components. Procedia CIRP 2013, 6, 368-372.

26. De Silva, A. K. M.; Altena, H. S. J.; McGeough, J. A., Influence of Electrolyte Concentration on Copying Accuracy of Precision-ECM. CIRP Annals 2003, 52 (1), 165-168.

27. Chun, K. H.; Kim, S. H.; Lee, E. S., Analysis of the relationship between electrolyte characteristics and electrochemical machinability in PECM on invar (Fe-Ni) fine sheet. The International Journal of Advanced Manufacturing Technology 2016, 87 (9), 3009-3017.

Mis en ligne le 3 janvier 2020 par Journal of Applied Electrochemistry
https://doi.org/10.1007/s10800-019-01386-z